# Band structure analysis of leaky Bloch waves in 2D phononic crystal plates

Matteo Mazzotti[a,*], Marco Miniaci[b], Ivan Bartoli[a]

[a] *Civil, Architectural & Environmental Engineering Department, Drexel University, 3141 Chestnut St, Philadelphia, PA 19104, USA*
[b] *University of Le Havre, Laboratoire Ondes et Milieux Complexes, UMR CNRS 6294, 75 Rue Bellot, 76600 Le Havre, France*

**Abstract**

A hybrid Finite Element-Plane Wave Expansion method is presented for the band structure analysis of phononic crystal plates with two dimensional lattice that are in contact with acoustic half-spaces. The method enables the computation of both real (propagative) and imaginary (attenuation) components of the Bloch wavenumber at any given frequency.

Three numerical applications are presented: a benchmark dispersion analysis for an oil-loaded Titanium isotropic plate, the band structure analysis of a water-loaded Tungsten slab with square cylindrical cavities and a phononic crystal plate composed of Aurum cylinders embedded in an epoxy matrix.

*Keywords:* phononic crystals, leaky Bloch waves, attenuation, band structure, finite element method, plane wave expansion method

## 1. Introduction

Over the past two decades, propagation of elastic waves in phononic crystal (PC) plates has attracted much attention due to their unique dynamic properties such as negative refraction [1], stop-band filtering [2], cloaking [3], among the other unconventional properties. PC plates are generally made of periodically distributed inclusions in a hosting material (matrix) and, depending on the

*Corresponding author
*Email address:* matteo.mazzotti@drexel.edu (Matteo Mazzotti)

physical nature of the components, can be classified in solid-solid, fluid-fluid and mixed solid-fluid composite systems [4].

In normal ambient conditions, the atmosphere surrounding the PC plate does not induce significant radiation of energy due to the high impedance mismatch at the solid-fluid interface. Therefore, such systems are treated as being in vacuum. However, PC plates surrounded by heavier fluids require mathematical models with appropriate radiation boundary conditions. Although a number of theoretical and experimental studies can be found in literature for the band-structure analysis of PC plates immersed in vacuum [4, 5], their fluid-loaded counterparts seem to have received minor attention. Early studies in this sense are represented by the works of Mace [6], Eatwell [7] and Mead [8], who investigated the radiation properties of fluid-loaded plates stiffened along one principal direction. More recently, different formulations have been proposed in which half-spaces have been modelled by means of analytical methods [9] as well as Finite Element (FEM)-based absorbing regions [10, 11, 12] and Perfectly Matched Layers [13, 14], while the so-called Plane Wave Expansion (PWE) method has been used in [15, 16, 17].

The main goal behind the present paper is to develop a coupled FEM-PWE method which enables the computation of the complex wavenumber-frequency band diagram for elastic PC plates with inclusions of arbitrary shape that are in contact with perfect fluids. The proposed formulation has the major advantage of avoiding spurious modes typical of numerical methods based on a finite discretization of the semi-infinite medium. Moreover, it can be extended to the case of lossy materials. However, the method cannot be applied to the case of a PC plate with a unit cell involving different material types such as fluid and solids. In order to benchmark the method, a fluid-loaded homogeneous isotropic plate is first examined, while the band structures for the real and imaginary components of the Bloch wavenumber are shown for a 1D PC and a 2D PC plate.

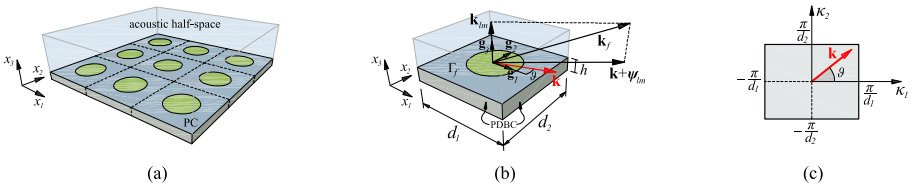


Figure 1: PC plate model with acoustic half-space (a), primitive cell (b) and corresponding 2D reciprocal lattice (c).

## 2. Hybrid Finite Element-Plane Wave Expansion (FEM-PWE) method

In this section, a hybrid variational formulation is described for the PC plate of Fig. 1 with $d_1$- and $d_2$-periodicity along directions 1 and 2, respectively, thickness $h$ and density $\rho$. The plate is in contact along the surface $\Gamma_f$ with a perfect fluid of density $\rho_f$ and sound speed $c_f$ that is infinitely extended along the direction 3. The domain of the primitive solid cell is denoted by $V = \Omega h$, where $\Omega = |d_1\mathbf{g}_1 \times d_2\mathbf{g}_2|$ while $\mathbf{g}_j$ represents the unit vector in the $j$-th direction.

By means of Bloch's theorem, the displacement in the solid PC and pressure in the fluid are given by $\mathbf{u}(\mathbf{x},t) = \tilde{\mathbf{u}}(\mathbf{x},t)\exp[\mathrm{i}(\mathbf{k}^{\mathrm{T}}\mathbf{x} - \omega t)]$ and $p(\mathbf{x},t) = \tilde{p}(\mathbf{x},t)\exp[\mathrm{i}(\mathbf{k}^{\mathrm{T}}\mathbf{x} - \omega t)]$, respectively, where i is the imaginary unit, $t$ is time, $\omega$ denotes the angular frequency, $\mathbf{x} = [x_1, x_2, x_3]^{\mathrm{T}}$ is the configuration vector, $\tilde{\mathbf{u}}(\mathbf{x},t) = [\tilde{u}_1, \tilde{u}_2, \tilde{u}_3]^{\mathrm{T}}$ and $\tilde{p}(\mathbf{x},t)$ are $\Omega$-periodic functions while $\mathbf{k} = [\kappa_1, \kappa_2, 0]^{\mathrm{T}} = \kappa\mathbf{\Phi}(\vartheta)$ is the Bloch wavevector, being $\mathbf{\Phi}(\vartheta) = [\cos\vartheta, \sin\vartheta, 0]^{\mathrm{T}}$ and $\vartheta$ its orientation angle with respect to the axis $x_1$.

Following a procedure similar to that outlined in [5] and accounting for the virtual work on the plate from the external fluid, a variational formulation for the solid PC can be stated as (the time dependency being dropped for conciseness)

$$-\int_V \rho(\mathbf{x})\omega^2 \left(\delta\tilde{\mathbf{u}}(\mathbf{x})\right)^{\mathrm{H}} \tilde{\mathbf{u}}(\mathbf{x})\mathrm{d}v + \int_V \left(\delta\mathbf{e}(\mathbf{x},\vartheta)\right)^{\mathrm{H}} \mathbf{C}(\mathbf{x})\mathbf{e}(\mathbf{x},\vartheta)\mathrm{d}v - \int_{\Gamma_f} \left(\delta\tilde{\mathbf{u}}(\mathbf{x})\right)^{\mathrm{H}} \tilde{p}(\mathbf{x})\mathbf{n}_3\mathrm{d}s = 0, \tag{1}$$

where $\mathbf{C}(\mathbf{x}) = C_{ijkl}(\mathbf{x})$ denotes the fourth order elasticity tensor, $\mathbf{e}(\mathbf{x},\vartheta) = \sum_{j=1}^{3} \mathbf{L}_j[\partial/\partial x_j + \mathrm{i}\kappa\mathbf{\Phi}(\vartheta)\mathbf{g}_j^{\mathrm{T}}]\tilde{\mathbf{u}}(\mathbf{x})$ indicates the Bloch strain vector, in which

$\mathbf{L}_j$ are compatibility operators defined in [18]-Eq. (8) while $\mathbf{n}_3$ ($= \pm\mathbf{g}_3$) is the outward normal at $\mathbf{x} \in \Gamma_f$.

Eq. (1) is discretized via a standard finite element discretization scheme for the solid PC, while the Plane Wave Expansion method [19, 20] is used to represent the wave field in the acoustic half-space. Accordingly, the displacement field at $\mathbf{x} \in V \cup \Gamma_f$ is interpolated as $\tilde{\mathbf{u}}(\mathbf{x}) = \mathbf{N}(\mathbf{x})\tilde{\mathbf{q}}(\mathbf{x})$, where $\mathbf{N}(\mathbf{x})$ is a matrix of polynomial shape functions and $\tilde{\mathbf{q}}(\mathbf{x})$ denotes the vector of nodal displacements. The pressure field is expanded as $p(\mathbf{x}) = \sum_{l,m=-\infty}^{+\infty} A_{lm}\exp[\mathrm{i}(\mathbf{k}+\boldsymbol{\psi}_{lm})^{\mathrm{T}}\mathbf{x}]$, where $A_{lm} = P_{lm}\exp(\mathrm{i}\kappa_{lm}\mathbf{g}_3^{\mathrm{T}}\mathbf{x})$ and $\boldsymbol{\psi}_{lm} = [2\pi l/d_1, 2\pi m/d_2, 0]^{\mathrm{T}}$, being $P_{lm}$ an unknown complex wave amplitude and $\kappa_{lm} = |\mathbf{k}_{lm}| = \pm[\kappa_f^2 - (\mathbf{k}+\boldsymbol{\psi}_{lm})^{\mathrm{T}}(\mathbf{k}+\boldsymbol{\psi}_{lm})]^{1/2}$, in which $\kappa_f = |\mathbf{k}_f| = \omega/c_f$ is the fluid wavenumber. By enforcing the continuity equation $\partial p(\mathbf{x})/\partial \mathbf{n}_3|_{\Gamma_f} = -\omega^2\rho_f \mathbf{n}_3^{\mathrm{T}}\mathbf{u}(\mathbf{x})$ on the fluid-solid interface and using orthogonality, the Bloch pressure and normal displacement mode functions can be expressed respectively in the form

$$\tilde{p}(\mathbf{x}) = \sum_{l,m=-\infty}^{+\infty} A_{lm}\exp\left(\mathrm{i}\boldsymbol{\psi}_{lm}^{\mathrm{T}}\mathbf{x}\right), \tag{2}$$

$$-\omega^2\rho_f \mathbf{n}_3^{\mathrm{T}}\tilde{\mathbf{u}}(\mathbf{x}) = \sum_{l,m=-\infty}^{+\infty} \mathrm{i}\kappa_{lm}A_{lm}\exp\left(\mathrm{i}\boldsymbol{\psi}_{lm}^{\mathrm{T}}\mathbf{x}\right). \tag{3}$$

The Fourier coefficients in Eq. (3) are given by

$$A_{lm}(\omega,\vartheta) = -\frac{\mathrm{i}\rho_f\omega^2}{\kappa_{lm}(\omega,\vartheta)\Omega}\int_{\Gamma_f} \mathbf{n}_3^{\mathrm{T}}\tilde{\mathbf{u}}(\mathbf{x})\exp\left(-\mathrm{i}\boldsymbol{\psi}_{lm}^{\mathrm{T}}\mathbf{x}\right)\,\mathrm{d}s. \tag{4}$$

Incorporating Eq. (4) into Eq. (2), substituting the resulting expression into Eq. (1) and applying a standard finite element assembling procedure over the $(1,..,e,..,N_e)$ elements of the mesh results in the following system of equations:

$$\left\{\kappa^2\mathbf{K}_3(\vartheta) + \mathrm{i}\kappa\left[\mathbf{K}_2(\vartheta) - (\mathbf{K}_2(\vartheta))^{\mathrm{T}}\right] + \mathbf{K}_1(\vartheta) - \omega^2\left[\mathbf{M} + \frac{\mathrm{i}\rho_f}{\Omega}\sum_{l,m=-\infty}^{+\infty}\frac{\mathbf{W}_{lm}\mathbf{W}_{lm}^{\mathrm{H}}}{\kappa_{lm}(\omega,\vartheta)}\right]\right\}\tilde{\mathbf{Q}}(\omega,\vartheta) = \mathbf{0}, \tag{5}$$

where $\tilde{\mathbf{Q}}(\omega,\vartheta) = \bigcup_e \tilde{\mathbf{q}}_e(\omega,\vartheta)$ is the global vector of nodal displacements, $\bigcup_e$ denotes the assembling operation and

| | $\mathrm{Re}(\mathbf{k}+\boldsymbol{\psi}_{lm})\cdot\mathrm{Im}(\mathbf{k}+\boldsymbol{\psi}_{lm})=0$ | $\mathrm{Re}(\mathbf{k}+\boldsymbol{\psi}_{lm})\cdot\mathrm{Im}(\mathbf{k}+\boldsymbol{\psi}_{lm})>0$ | $\mathrm{Re}(\mathbf{k}+\boldsymbol{\psi}_{lm})\cdot\mathrm{Im}(\mathbf{k}+\boldsymbol{\psi}_{lm})<0$ |
|---|---|---|---|
| $\lvert\mathrm{Re}(\mathbf{k}+\boldsymbol{\psi}_{lm})\rvert<\kappa_f$ | $\mathrm{Re}(\kappa_{lm})>0$ | $\mathrm{Im}(\kappa_{lm})<0$ | $\mathrm{Im}(\kappa_{lm})>0$ |
| $\lvert\mathrm{Re}(\mathbf{k}+\boldsymbol{\psi}_{lm})\rvert>\kappa_f$ | $\mathrm{Im}(\kappa_{lm})>0$ | $\mathrm{Im}(\kappa_{lm})>0$ | $\mathrm{Im}(\kappa_{lm})>0$ |

Table 1: Physical choices of $\mathrm{sgn}(\kappa_{lm})$, corresponding to pressure wave fields exponentially decaying ($\mathrm{Im}(\kappa_{lm})>0$) and growing ($\mathrm{Im}(\kappa_{lm})<0$) at infinity along direction 3 [22].

$$\mathbf{K}_1(\vartheta)=\bigcup_e\int_{V_e}\sum_{j=1}^{3}\frac{\partial\left(\mathbf{N}(\mathbf{x})\right)^{\mathrm{T}}}{\partial x_j}\mathbf{L}_j^{\mathrm{T}}\mathbf{C}_e(\mathbf{x})\mathbf{L}_j\frac{\partial\mathbf{N}(\mathbf{x})}{\partial x_j}\,\mathrm{d}v, \tag{6}$$

$$\mathbf{K}_2(\vartheta)=\bigcup_e\int_{V_e}\sum_{j=1}^{3}\left(\mathbf{N}(\mathbf{x})\right)^{\mathrm{T}}\mathbf{g}_j\left(\boldsymbol{\Phi}(\vartheta)\right)^{\mathrm{T}}\mathbf{L}_j^{\mathrm{T}}\mathbf{C}_e(\mathbf{x})\mathbf{L}_j\frac{\partial\mathbf{N}(\mathbf{x})}{\partial x_j}\,\mathrm{d}v, \tag{7}$$

$$\mathbf{K}_3(\vartheta)=\bigcup_e\int_{V_e}\sum_{j=1}^{3}\left(\mathbf{N}(\mathbf{x})\right)^{\mathrm{T}}\mathbf{g}_j\left(\boldsymbol{\Phi}(\vartheta)\right)^{\mathrm{T}}\mathbf{L}_j^{\mathrm{T}}\mathbf{C}_e(\mathbf{x})\mathbf{L}_j\boldsymbol{\Phi}(\vartheta)\mathbf{g}_j^{\mathrm{T}}\mathbf{N}(\mathbf{x})\,\mathrm{d}v, \tag{8}$$

$$\mathbf{M}=\bigcup_e\int_{V_e}\left(\mathbf{N}(\mathbf{x})\right)^{\mathrm{T}}\rho_e(\mathbf{x})\mathbf{N}(\mathbf{x})\,\mathrm{d}v, \tag{9}$$

$$\mathbf{W}_{lm}=\bigcup_e\int_{\partial V_e\in\Gamma_f}\left(\mathbf{N}(\mathbf{x})\right)^{\mathrm{T}}\mathbf{n}_3\exp\left(\mathrm{i}\boldsymbol{\psi}_{lm}^{\mathrm{T}}\mathbf{x}\right)\,\mathrm{d}s. \tag{10}$$

It is remarked that, in order to obey periodicity, Eq. (5) must be subjected to appropriate periodic Dirichlet boundary conditions (PDBC) on the lateral boundaries of the cell (see [5, 20] for further details).

Eq. (5) is configured as a nonlinear eigenvalue problem in the complex Bloch wavenumber $\kappa(\omega,\vartheta)$ for any fixed real positive frequency $\omega$ and assigned orientation $\vartheta\in[0,2\pi]$, and it is solved in the present work by means of a contour integral algorithm [21]. It should be noted that, while the real components of $\mathbf{k}(\omega,\vartheta)$ are restricted to the first Brillouin zone ($-\pi/d_j\le\mathrm{Re}(\kappa_j(\omega,\vartheta))\le\pi/d_j$, $j=1,2$), the imaginary components, describing the wave decay in space along the corresponding directions, are unbounded.

Of fundamental importance in the solution of the dispersion equation is the determination of the correct sign of $\kappa_{lm}$, which is a two-valued function of the Bloch wavenumber $\kappa(\omega,\vartheta)$. The choices of $\mathrm{sgn}(\kappa_{lm})$ with physical meaning depend on the behaviour of the spatial harmonic $(l,m)$ in the acoustic region [22] and are listed in Table 1.

## 3. Numerical applications

In order to validate the proposed method, a benchmark analysis is first proposed for a homogeneous Titanium plate ($\rho = 4460$ kg/m$^3$, $C_{11} = 163.8$ GPa, $C_{12} = 70.73$ GPa, $C_{44} = 46.53$ GPa) of 10 mm thickness loaded with oil ($\rho_f =$ 870 kg/m$^3$, $c_f = 1740$ m/s) on one side. The corresponding real wavenumber and attenuation dispersion curves in the $0-500$ kHz frequency range are shown in Fig. 2(a), where the continuous blue line indicates the analytical solution computed using the software Disperse [23] while the red dots correspond to the numerical solution obtained with the proposed method using a cell of $10\times1\times10$ mm subdivided into 32 elements with quadratic shape functions (951 dofs), $\vartheta = 0$ and assuming ($l = -20:20$, $m = 0$).

It can be observed that the two sets of solutions are in very good agreement with the exception of the mode A0$''$, which is hard to compute by the proposed method at frequencies higher than 50 kHz due to numerical instabilities occurring when $\kappa_{lm}$ approaches $\kappa_f$. Further details on the physical behaviour of the various guided wave modes in the spectra can be found in [24, 25] and are omitted here for the sake of brevity.

In the second numerical application, the Tungsten phononic crystal slab ($\rho = 19200$ kg/m$^3$, $C_{11} = 502$ GPa, $C_{12} = 199$ GPa, $C_{44} = 152$ GPa) with embedded square cylindrical cavities presented in [26] is analyzed for the case of one side loaded by water ($\rho_f = 998$ kg/m$^3$, $c_f = 1478$ m/s). The external dimensions of the cell are $1\times0.1\times1$ mm, while the side length of the internal square cavity is equal to 0.3mm. The band structures for the in-vacuum (blue circles) and fluid-loaded (red dots) cases are shown in Fig. 2(b) in the $0-2$ MHz frequency range for a mesh of 128 elements with quadratic shape functions (3168 dofs), $\vartheta = 0$ and ($l = -20:20$, $m = 0$). In analogy with the fluid-loaded homogeneous plate, also in this case the antisymmetric mode A0 separates in two branches A0$'$ and A0$''$, with the first belonging to the Fast Wave Region (FWR) and thus radiating energy, while the second corresponds to a slow, non-attenuated wave. It should be noted that the presence of the fluid does not

substantially alter the propagation constants of the remaining modes in the spectra, with the original band gap in the $1.37 - 1.74$ MHz frequency range being preserved.

The third numerical experiment concerns a phononic crystal plate composed of Aurum cylinders ($\rho = 19300$ kg/m$^3$, $C_{11} = 192.5$ GPa, $C_{12} = 163$ GPa, $C_{44} = 42.4$ GPa) embedded in a epoxy matrix ($\rho = 1180$ kg/m$^3$, $C_{11} = 7.58$ GPa, $C_{12} = 4.42$ GPa, $C_{44} = 1.58$ GPa) and loaded with water on one side. The cell has dimensions $10 \times 10 \times 2.5$ mm with the radius of the Au cylinders equal to 0.3 mm, and is discretized by means of 216 elements with quadratic shape functions (3867 dofs).

The in-vacuum band structure for $\vartheta = 0$ can be found in Ref. [27]-Fig. 2 (corresponding to the $\Gamma - \mathrm{X}$ direction in the first Brillouin zone) and is here represented in Fig. 2(c) using blue circles, while the corresponding fluid-loaded case, obtained for ($l = -20 : 20$, $m = -20 : 20$), is represented by red dots. From the inspection of the band diagrams it appears that the presence of the fluid introduces some slight perturbations in the real component of the Bloch wavenumber for modes M1 and M4, the latter exhibiting moderate attenuations in the fast branch. The remaining radiating modes in the spectra are represented by modes M7 and M8. In particular, the M8 branch for the fluid-loaded case is not represented in the spectra since its attenuation values are comparable to those observed in the band gaps of the corresponding in-vacuum band diagram. It can also be noted that, although modes M5 and M6 present fast branches, their attenuation values in the FWR are close to zero due since they do not experience significant displacements in direction 3.

Of particular interest is the presence of the new mode M9 in the diagram, which propagates in the frequency range corresponding to the band gap of the in-vacuum case and corresponds to an interface and a bounded slow mode for values of frequency lower and higher than 52 kHz, respectively.

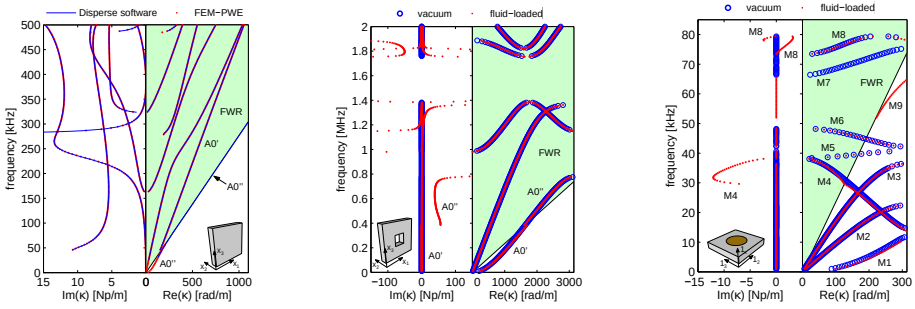


(a) (b) (c)

Figure 2: Dispersion curves of the oil-loaded Titanium plate (a) and band diagrams of the water-loaded Tungsten slab (b) and Aurum-epoxy phononic plate (c). The shaded areas correspond to the Fast Wave Regions (FWR).

## 4. Conclusions

A hybrid finite element-plane wave expansion method has been presented for the band diagrams calculation of fluid-loaded PC plates and benchmarked against analytical solutions available for homogeneous plates.

From the computed band diagram of a water-loaded 1D PC Tungsten slab with square cylindrical cavities, some analogies have been observed between the physical behaviour of leaky Bloch waves and guided waves in the homogeneous plate. The case of a water-loaded 2D PC plate made of Aurum cylinders embedded in a epoxy matrix has been also analyzed, for which a slow mode is observed in the band gap region of the corresponding in-vacuum case.

## 5. Acknowledgments

Marco Miniaci has received funding from the European Unions Horizon 2020 research and innovation program under the Marie Sk lodowska-Curie [grant number 658483].

## References


[1] B. Morvan, A. Tinel, A.-C. Hladky-Hennion, J. Vasseur, B. Dubus, Experimental demonstration of the negative refraction of a transverse elastic wave in a two-dimensional solid phononic crystal, Applied Physics Letters 96 (10). doi:http://dx.doi.org/10.1063/1.3302456.

[2] R. Martínez-Sala, J. Sancho, J. Sánchez, V. Gómez, J. Llinares, F. Meseguer, Sound attenuation by sculpture, Nature 378 (1995) 241. doi:http://dx.doi.org/10.1038/378241a0.

[3] D. Colquitt, M. Brun, M. Gei, A. Movchan, N. Movchan, I. Jones, Transformation elastodynamics and cloaking for flexural waves, Journal of the Mechanics and Physics of Solids 72 (2014) 131 – 143. doi:http://dx.doi.org/10.1016/j.jmps.2014.07.014.

[4] Y. Pennec, J. O. Vasseur, B. Djafari-Rouhani, L. Dobrzyński, P. A. Deymier, Two-dimensional phononic crystals: Examples and applications, Surface Science Reports 65 (8) (2010) 229 – 291. doi:http://dx.doi.org/10.1016/j.surfrep.2010.08.002.

[5] M. Collet, M. Ouisse, M. Ruzzene, M. Ichchou, Floquet-bloch decomposition for the computation of dispersion of two-dimensional periodic, damped mechanical systems, International Journal of Solids and Structures 48 (20) (2011) 2837 – 2848. doi:http://dx.doi.org/10.1016/j.ijsolstr.2011.06.002.

[6] B. Mace, Periodically stiffened fluid-loaded plates, i: Response to convected harmonic pressure and free wave propagation, Journal of Sound and Vibration 73 (4) (1980) 473 – 486. doi:http://dx.doi.org/10.1016/0022-460X(80)90662-8.

[7] G. Eatwell, Free-wave propagation in an irregularly stiffened, fluid-loaded plate, Journal of Sound and Vibration 88 (4) (1983) 507 – 522. doi:http://dx.doi.org/10.1016/0022-460X(83)90653-3.

[8] D. J. Mead, Plates with regular stiffening in acoustic media: Vibration and radiation, The Journal of the Acoustical Society of America 88 (1) (1990) 391–401. doi:http://dx.doi.org/10.1121/1.399915.

[9] L. C. Botten, N. A. Nicorovici, R. C. McPhedran, C. M. d. Sterke, A. A. Asatryan, Photonic band structure calculations using scattering matrices, Phys. Rev. E 64 (2001) 046603. doi:10.1103/PhysRevE.64.046603.

[10] H. Estrada, P. Candelas, F. Belmar, A. Uris, F. J. García de Abajo, F. Meseguer, Engineering surface waves in flat phononic plates, Phys. Rev. B 85 (2012) 174301. doi:10.1103/PhysRevB.85.174301.

[11] R. P. Moiseyenko, N. F. Declercq, V. Laude, Guided wave propagation along the surface of a one-dimensional solidfluid phononic crystal, Journal of Physics D: Applied Physics 46 (36) (2013) 365305. doi:http://dx.doi.org/10.1088/0022-3727/46/36/365305.

[12] B. Graczykowski, F. Alzina, J. Gomis-Bresco, C. M. Sotomayor Torres, Finite element analysis of true and pseudo surface acoustic waves in one-dimensional phononic crystals, Journal of Applied Physics 119 (2). doi:http://dx.doi.org/10.1063/1.4939825.

[13] A. Khelif, Y. Achaoui, S. Benchabane, V. Laude, B. Aoubiza, Locally resonant surface acoustic wave band gaps in a two-dimensional phononic crystal of pillars on a surface, Phys. Rev. B 81 (2010) 214303. doi:10.1103/PhysRevB.81.214303.

[14] M. Molerón, S. Félix, V. Pagneux, O. Richoux, Sound propagation in periodic urban areas, Journal of Applied Physics 111 (11). doi:http://dx.doi.org/10.1063/1.4725487.

[15] A. A. Maznev, A. G. Every, Surface acoustic waves in a periodically patterned layered structure, Journal of Applied Physics 106 (11). doi:http://dx.doi.org/10.1063/1.3267290.

[16] P. Graczyk, B. Mroz, Simulations of acoustic waves bandgaps in a surface of silicon with a periodic hole structure in a thin nickel film, AIP Advances 4 (7). doi:http://dx.doi.org/10.1063/1.4892076.

[17] T. Weisser, J.-P. Groby, O. Dazel, F. Gaultier, E. Deckers, S. Futatsugi, L. Monteiro, Acoustic behavior of a rigidly backed poroelastic layer with periodic resonant inclusions by a multiple scattering approach, The Journal of the Acoustical Society of America 139 (2) (2016) 617–629. doi:http://dx.doi.org/10.1121/1.4940669.

[18] M. Mazzotti, I. Bartoli, A. Marzani, E. Viola, A coupled safe-2.5d bem approach for the dispersion analysis of damped leaky guided waves in embedded waveguides of arbitrary cross-section, Ultrasonics 53 (7) (2013) 1227 – 1241. doi:http://dx.doi.org/10.1016/j.ultras.2013.03.003.

[19] A. Hladky-Hennion, J. Decarpigny, Analysis of the scattering of a plane acoustic wave by a doubly periodic structure using the finite element method: Application to alberich anechoic coatings, The Journal of the Acoustical Society of America 90 (6) (1991) 3356–3367. doi:http://dx.doi.org/10.1121/1.401395.

[20] J. A. Kulpe, K. G. Sabra, M. J. Leamy, A three-dimensional bloch wave expansion to determine external scattering from finite phononic crystals, The Journal of the Acoustical Society of America 137 (6) (2015) 3299–3313. doi:http://dx.doi.org/10.1121/1.4921548.

[21] W.-J. Beyn, An integral method for solving nonlinear eigenvalue problems, Linear Algebra and its Applications 436 (10) (2012) 3839 – 3863, special Issue dedicated to Heinrich Voss's 65th birthday. doi:http://dx.doi.org/10.1016/j.laa.2011.03.030.

[22] P. Baccarelli, S. Paulotto, C. D. Nallo, Full-wave analysis of bound and leaky modes propagating along 2d periodic printed structures with arbitrary metallisation in the unit cell,

IET Microwaves, Antennas Propagation 1 (1) (2007) 217–225. doi:http://dx.doi.org/10.1049/iet-map:20050321.

[23] I. C. London, Disperse, Ver. 2.0.20a (2013).

[24] H. Gravenkamp, C. Birk, C. Song, Numerical modeling of elastic waveguides coupled to infinite fluid media using exact boundary conditions, Computers & Structures 141 (2014) 36 – 45. doi:http://dx.doi.org/10.1016/j.compstruc.2014.05.010.

[25] T. Hayashi, D. Inoue, Calculation of leaky lamb waves with a semi-analytical finite element method, Ultrasonics 54 (6) (2014) 1460 – 1469. doi:http://dx.doi.org/10.1016/j.ultras.2014.04.021.

[26] J. Chen, Y. Xia, X. Han, H. Zhang, Lamb waves in phononic crystal slabs: Truncated plane parallels to the axis of periodicity, Ultrasonics 52 (7) (2012) 920 – 924. doi:http://dx.doi.org/10.1016/j.ultras.2012.02.015.

[27] J.-C. Hsu, T.-T. Wu, Efficient formulation for band-structure calculations of two-dimensional phononic-crystal plates, Phys. Rev. B 74 (2006) 144303. doi:10.1103/PhysRevB.74.144303.